Available online at www.sciencedirect.com
SCIENCE DIRECT®
Journal of Computational Physics 188 (2003) 524–542
JOURNAL OF COMPUTATIONAL PHYSICS
www.elsevier.com/locate/jcp

On the dissipation mechanism of Godunov-type schemes

Soo Hyung Park *, Jang Hyuk Kwon

Department of Aerospace Engineering, Korea Advanced Institute of Science and Technology, 371-1 Guseong-Dong, Yuseong-Gu, Daejeon 305-701, Republic of Korea

Received 3 April 2001; received in revised form 7 October 2002; accepted 21 October 2002

Abstract

Dissipation mechanisms of Godunov-type schemes are presented in the framework of unified representation. The causes of inaccuracy at the contact discontinuity and the dissipation mechanism in the numerical mass flux of the HLLEM scheme are examined first. A ''vacuum preserving property'' is defined and the prominent role of the numerical signal speed involved with the rarefaction waves in the expanding region is analyzed. Through a linear perturbation analysis on the odd–even decoupling problem, necessary conditions for designing a shock stable scheme are discussed. As a result, an improved HLLE(HLLE+) scheme is proposed and its dissipation mechanism is analyzed. The diffusivity of the Godunov-type schemes is examined by two-dimensional hypersonic viscous flow.

Keywords: Godunov-type schemes; Contact discontinuity; Vacuum preserving property; Shock instability; HLLE+ scheme

1. Introduction

A number of numerical flux functions for inviscid fluxes have been devised as approximate solutions to the Riemann problem. Approximate Riemann solvers such as Roe's [1] and Osher–Solomon's schemes [2] are widely used for compressible flows because of their mathematical clarity and high quality resolution. However, the schemes often encounter catastrophic solutions, for example, nonphysical expansion shocks and nonpositive solutions or shock instability, namely the carbuncle. Even the Godunov's exact Riemann solver [3] has deficiencies in certain conditions.

Harten et al. [4] suggested a mathematical theory of the upstream difference scheme and the Godunov-type scheme, denoted by the Harten–Lax–van Leer (HLL) which approximates the solution of Riemann problem with two signal waves. A typical example of the HLL solver is the HLLE scheme [5] which proposed the bounds of signal waves by using the eigenvalues of Roe matrix to satisfy the entropy and the positivity conditions. Despite its desirable properties, it is difficult to simulate practical problems because of its highly dissipative behavior. The HLLE-Modified (HLLEM) scheme [6] enhances the resolution com-

* Corresponding author.
E-mail addresses: pish@kaist.ac.kr (S.H. Park), jhkwon@kaist.ac.kr (J.H. Kwon).

0021-9991/03/$ - see front matter
doi:10.1016/S0021-9991(03)00191-8

parable to that of the Roe scheme. However, several problems have been reported for this scheme [7,8]. The two main problems of the Godunov-type schemes are multidimensional shock instability and the nonexistence of strong receding flows [9]. It has also been found that the HLLEM which recovers the information of contact discontinuity [10] is less accurate than the Roe.

Our main attention is to understand the causes of the breakdowns and the inaccuracies of the HLLEM scheme. It is useful to unify the Godunov-type schemes by using control parameters in order to identify their numerical dissipation mechanism. The unified approach enables us to obtain important information about the accuracy and the robustness. Linear discrete analysis [9,11] is performed to study the dissipation mechanism.

In this paper, it is shown that the mechanism of the HLLEM scheme accompanies somewhat erroneous dissipation and the Liou's lemma [9] for the contact discontinuity can be successfully applied to check the accuracy of a numerical flux function. We also claim that the dissipative solutions of the HLLE and the HLLEM schemes for strong receding flows result from the numerical momentum fluxes rather than the mass flux. According to our analysis for odd–even decoupling, the derived condition shows that the Liou's lemma, which is defined by "A scheme having the property $D^{(p)} = 0$ in the mass flux is a shock-stable scheme," is only a sufficient condition for a shock-stable scheme. This is important in designing new and improved schemes [12]. To verify the analysis, the shock tube problems and the boundary layer problems are considered.

This paper is organized as follows: In Section 2, we describe the formulations of the Godunov-type schemes and represent those schemes in a unified form. The numerical meaning of the entropy corrections to the Roe scheme is given. Section 3 is then devoted to the analysis of the numerical dissipation mechanism of the Godunov-type schemes. The instabilities of the schemes are analyzed in detail. In Section 4, an improved HLLE(HLLE+) scheme is proposed from the analysis. The wall heat fluxes for the hypersonic viscous flows are computed to demonstrate the effect of the numerical dissipation since the computed heat fluxes are very sensitive to the dissipation mechanism. Conclusions are drawn in Section 5.

2. Unified Godunov-type schemes

We consider the conservative form of the two-dimensional (2-D) compressible Navier–Stokes equations,

$$\frac{\partial \mathbf{w}}{\partial t} + \frac{\partial \mathbf{f}}{\partial x} + \frac{\partial \mathbf{g}}{\partial y} = \frac{\partial \mathbf{f}_v}{\partial x} + \frac{\partial \mathbf{g}_v}{\partial y}, \tag{1}$$

where the conservative flow variable $\mathbf{w} = [\rho, \rho u, \rho v, \rho e]^T$. $\mathbf{f}$ and $\mathbf{g}$ are the inviscid fluxes in x and y directions respectively, and $\mathbf{f}_v$ and $\mathbf{g}_v$ are the viscous fluxes:

$$\mathbf{f} = \begin{bmatrix} \rho u \\ \rho u^2 + p \\ \rho uv \\ \rho uH \end{bmatrix}, \quad \mathbf{g} = \begin{bmatrix} \rho v \\ \rho uv \\ \rho v^2 + p \\ \rho vH \end{bmatrix}, \tag{2}$$

$$\mathbf{f}_v = \begin{bmatrix} 0 \\ \sigma_{xx} \\ \sigma_{xy} \\ u\sigma_{xx} + v\sigma_{xy} - q_x \end{bmatrix}, \quad \mathbf{g}_v = \begin{bmatrix} 0 \\ \sigma_{xy} \\ \sigma_{yy} \\ u\sigma_{yx} + v\sigma_{yy} - q_y \end{bmatrix}. \tag{3}$$

Here ρ and p are the density and pressure, u and v are the Cartesian velocity components. e is the total energy and $H = e + p/\rho$ is the total enthalpy. The quantity σ_{ij} and q_i are the viscous stresses and heat fluxes in x and y directions.

Numerical flux functions have been constructed for one-dimensional (1-D) Euler equations since the viscous fluxes can be discretized by the central differencing. Eq. (1) can be integrated cell-wise in 1-D space domain, then the discretized governing equation yields in conservation form

$$\mathbf{w}_i^{n+1} = \mathbf{w}_i^n - \frac{\Delta t}{\Delta x}(\mathbf{f}_{i+1/2}^n - \mathbf{f}_{i-1/2}^n). \tag{4}$$

The HLL Riemann solver [4] approximates the solution of Riemann problem with two waves propagating at speeds of b^r and b^l, as shown in Fig. 1. They are the lower and upper bounds for the physical signal speeds with which the information of the initial discontinuity is transported. To satisfy the entropy and the positivity conditions, Einfeldt [5] suggested adequate bounds by making use of the Roe-averaged eigenvalues, $\hat{\lambda}_p = \{\hat{u}, \hat{u} + \hat{a}, \hat{u} - \hat{a}, \hat{u}\}$, where $\hat{a}$ is the speed of sound at the cell interface and the subscript $p = 1, 2, 3, 4$. The superscript $\hat{}$ denotes the Roe-averaged values throughout this paper. Then the approximate signal speeds at the right and the left cell faces are defined to be:

$$b^r = \max\{\hat{\lambda}_2, u_r + a_r\}, \quad b^l = \min\{\hat{\lambda}_3, u_l - a_l\}. \tag{5}$$

Using this signal speeds, the HLLE scheme can be written by

$$\mathbf{f}^{\mathrm{HLLE}}(\mathbf{w}_l, \mathbf{w}_r) = \frac{b^+\mathbf{f}(\mathbf{w}_l) - b^-\mathbf{f}(\mathbf{w}_r)}{b^+ - b^-} + \frac{b^+ b^-}{b^+ - b^-}\{(\mathbf{w}_r - \mathbf{w}_l)\} \tag{6}$$

with $b^+ = \max\{b^r, 0.0\}, b^- = \min\{b^l, 0.0\}$. The HLLE scheme does not violate the positivity and the entropy conditions nor suffer instability at strong shocks. However, the contact discontinuities are smeared out excessively since it is very dissipative regardless of the chosen bounds.

The HLLEM scheme [6] improves the resolution of contact discontinuity by reusing the information of contact discontinuity in terms of modifying the intermediate state. The numerical flux function of the HLLEM scheme can then be written by

$$\mathbf{f}^{\mathrm{HLLEM}}(\mathbf{w}_l, \mathbf{w}_r) = \mathbf{f}^{\mathrm{HLLE}}(\mathbf{w}_l, \mathbf{w}_r) - \frac{b^+ b^-}{b^+ - b^-} \sum_{p=1,4} \bar{\delta}\alpha^p \mathbf{R}^p, \tag{7}$$

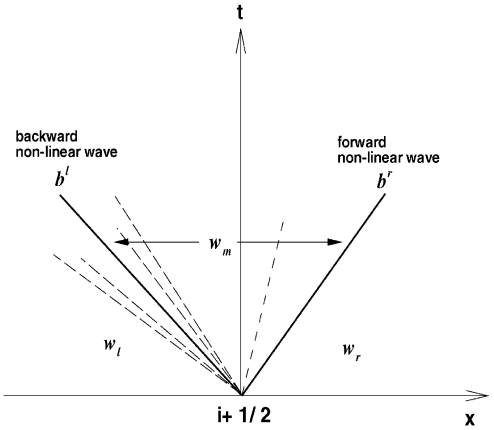

Fig. 1. The approximate solution of HLL Riemann solver.

where $\mathbf{R}^p (p = 1, 2, 3, 4)$ are the right eigenvectors of the flux Jacobian evaluated at the intermediate states. α^p are the coefficients of the projection of $\mathbf{w}_r - \mathbf{w}_l$ onto $\mathbf{R}^p$

$$\mathbf{w}_r - \mathbf{w}_l = \sum_{p=1}^{4} \alpha^p \mathbf{R}^p. \tag{8}$$

Since b^+ and b^- are positive and negative quantities, respectively, the last term in Eq. (7) is of an anti-diffusive nature. The anti-diffusion coefficient $\bar{\delta}$ is defined such that they can take out excess dissipation in the linear degenerated fields

$$\bar{\delta} = \frac{\hat{a}}{|\bar{u}| + \hat{a}}, \tag{9}$$

where the speed $\bar{u}$ is defined as the approximate speed of the contact discontinuity.

The above described schemes can be unified and characterized by using control parameters. This enables us to analyze the dissipation mechanisms of each scheme. The numerical flux $\mathbf{f}(\mathbf{w}_l, \mathbf{w}_r)$ of the unified Godunov-type schemes is defined by

$$\mathbf{f}(\mathbf{w}_l, \mathbf{w}_r) = \frac{b^+ \mathbf{f}(\mathbf{w}_l) - b^- \mathbf{f}(\mathbf{w}_r)}{b^+ - b^-} + \frac{b^+ b^-}{b^+ - b^-} \left\{ (\mathbf{w}_r - \mathbf{w}_l) - \sum_{p=1,4} \bar{\delta} \alpha^p \mathbf{R}^p \right\} \tag{10}$$

with b^r and b^l defined to be

$$b^r = \max\{\hat{\lambda}_2, \mathbf{C}^+\}, \quad b^l = \min\{\hat{\lambda}_3, \mathbf{C}^-\}. \tag{11}$$

According to the definition of $\mathbf{C}^+$, $\mathbf{C}^-$ and $\bar{u}$, different dissipation mechanisms can be described as follows:

HLLE

$$\mathbf{C}^+ = u_r + a_r, \quad \mathbf{C}^- = u_l - a_l, \quad |\bar{u}| = \infty \text{ so that } \bar{\delta} = 0.0. \tag{12}$$

HLLEM

$$\mathbf{C}^+ = u_r + a_r, \quad \mathbf{C}^- = u_l - a_l, \quad |\bar{u}| = \left| \frac{b^r + b^l}{2} \right|. \tag{13}$$

Roe

$$\mathbf{C}^+ = \hat{\lambda}_2, \quad \mathbf{C}^- = \hat{\lambda}_3, \quad |\bar{u}| = |\hat{u}|. \tag{14}$$

The Roe scheme can lead to a nonphysical solution with entropy-violating discontinuities, since no rarefaction waves are considered. Hence additional dissipation is required with nonlinear acoustic waves. On the other hand, no dissipation to linear contact waves results in instabilities in the transverse direction to a strong normal shock. It is possible to suppress them by using the entropy correction to linear waves. In this paper, Harten's and Lin's [13,14] entropy correction functions are applied in order to add some dissipation. To describe the entropy correction, the numerical flux function of the original Roe scheme is written as

$$\mathbf{f}^{\mathrm{ROE}}(\mathbf{w}_l, \mathbf{w}_r) = \frac{1}{2}\{\mathbf{f}(\mathbf{w}_l) + \mathbf{f}(\mathbf{w}_r)\} + \frac{1}{2} \sum_{p=1}^{4} \Psi(\hat{\lambda}_p) \alpha^p \mathbf{R}^p. \tag{15}$$

Harten's function is expressed as

$$\Psi(\hat{\lambda}_p) = \begin{cases} |\hat{\lambda}_p| & \text{if } |\hat{\lambda}_p| > \epsilon, \\ \frac{1}{2}\left[\frac{\hat{\lambda}_p^2+\epsilon^2}{\epsilon}\right] & \text{otherwise,} \end{cases} \qquad \epsilon = \epsilon^*\left(|\hat{u}_n| + \hat{a}\right), \tag{16}$$

where ϵ^* is a constant between 0 and 0.25, and $\hat{u}_n$ is the contravariant velocity normal to the cell interface. Harten's dissipation is inadequate for viscous computations as ϵ^* increases, since the dissipation added to the linear waves gives an unreasonably thick boundary layer.

Lin used the pressure gradient to design the 2-D isotropic correction function which suppresses the shock instability and reduces the dissipation added. Lin's function is expressed as

$$\Psi(\hat{\lambda}_p) = \begin{cases} |\hat{\lambda}_p| & \text{if } |\hat{\lambda}_p| > \epsilon_p, \\ \frac{1}{2}\left[\frac{\hat{\lambda}_p^2+\epsilon_p^2}{\epsilon_p} + |\hat{\lambda}_p|\right] & \text{otherwise,} \end{cases} \qquad \begin{aligned} \epsilon_{1,4} &= \left(|\hat{u}_n| + \hat{a}\right)(k_3 k_p), \\ \epsilon_{2,3} &= \left(|\hat{u}_n| + \hat{a}\right)(k_1 + k_2 k_p), \end{aligned} \tag{17}$$

k_p adjusts the magnitude of the dissipation as a shock indicator in 2-D problems which is defined by

$$(k_p)_{ij} = 0.5\left(\left|\frac{P_{i+1,j} - 2P_{i,j} + P_{i-1,j}}{P_{i+1,j} + 2P_{i,j} + P_{i-1,j}}\right| + \left|\frac{P_{i,j+1} - 2P_{i,j} + P_{i,j-1}}{P_{i,j+1} + 2P_{i,j} + P_{i,j-1}}\right|\right). \tag{18}$$

Lin proposed the values of $k_1 = 0.25$, $k_2 = 5$ and $k_3 = 15$. See [14] for details. Lin's method works well in many situations for hypersonic viscous flows. However, it needs a special treatment to reduce the amount of dissipation in the supersonic regions of flows. It also has some problems involved with convergence. Although the convergence problem can be suppressed by the smoothing parameter k_2, it degrades the normal and oblique shock resolutions since the dissipation to the nonlinear waves is added.

3. Analysis on numerical dissipation mechanism

Linear discrete analysis is a powerful tool to study the behavior of any scheme at a specified condition. In this section, it will be shown that the dissipation mechanism of the HLLEM scheme accompanies erroneous diffusion at contact discontinuities. The dissipative behavior at the receding flow and the odd–even decoupling problem along with the discrete analysis will be considered also.

3.1. Numerical dissipation at contact discontinuity

Since a contact discontinuity is numerically equivalent to a limiting case of a viscous boundary layer, the accuracy of a numerical method for Navier–Stokes equations can be verified by the contact discontinuity problem. Fig. 2 displays the numerical results for the stationary contact discontinuity problem. The Roe scheme gives the exact solution for the stationary contact discontinuity. The HLLEM solution is somewhat diffused though the erroneous diffusion is smaller than that of the HLLE scheme. To verify this result, the laminar boundary layer on a flat plate at Mach number of 0.3 is computed with the second-order accurate Roe and HLLEM schemes using MUSCL higher order interpolation [15]. Similarly, Fig. 3 shows somewhat different resolution between the Roe and the HLLEM for this problem. Einfeldt [5] defined the

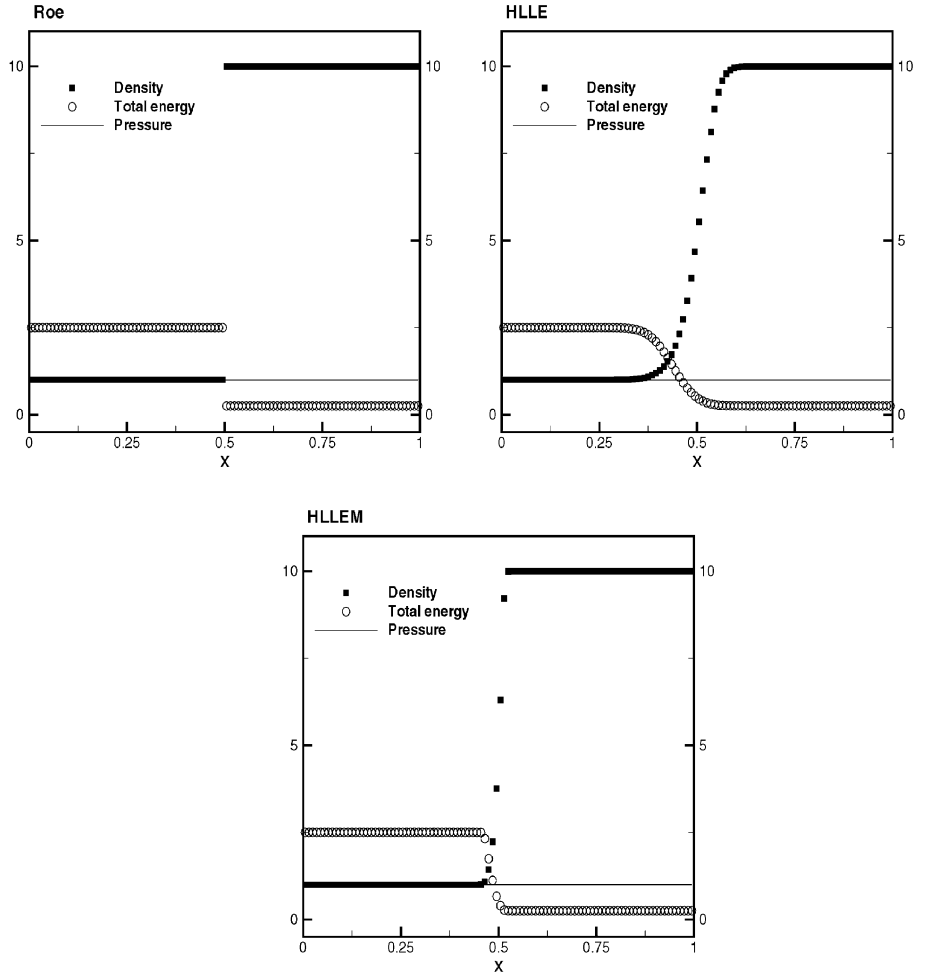

Fig. 2. Stationary contact discontinuity: $(\rho,u,p)_l=(1,0,1)$, $(\rho,u,p)_r=(10,0,1)$ at $x=0.5$.

approximate speed of contact discontinuity in Eq. (13) as the average of the largest and the smallest signal speeds. This approximation may lead to more dissipative solutions in the local Riemann problem.

Liou's lemma [9] has been thought to be a useful criterion for checking the accuracy of a numerical flux function involved with the contact discontinuity. The lemma requires the numerical mass flux function in Eq. (10) to be derived. The mass flux of the Godunov-type schemes, $\dot{\mathbf{m}}$, can be expressed as

$$\dot{\mathbf{m}}=\frac{1}{2}[(\rho u)_l+(\rho u)_r]-\frac{1}{2}D(\mathbf{w}_l,\mathbf{w}_r). \tag{19}$$

Here, $D(\mathbf{w}_l,\mathbf{w}_r)$ is the numerical dissipation term which can be expanded in terms of differences of variables (ρ,u,p)

$$D(\mathbf{w}_l,\mathbf{w}_r)=D^{(\rho)}\Delta\rho+D^{(u)}\Delta u+D^{(p)}\Delta p, \tag{20}$$

where $D^{(\rho)}$, $D^{(u)}$, and $D^{(p)}$ are the dissipation coefficients of $D(\mathbf{w}_l,\mathbf{w}_r)$. These coefficients are varied according to numerical schemes. Refer to [9] for further details in order to derive the coefficients.

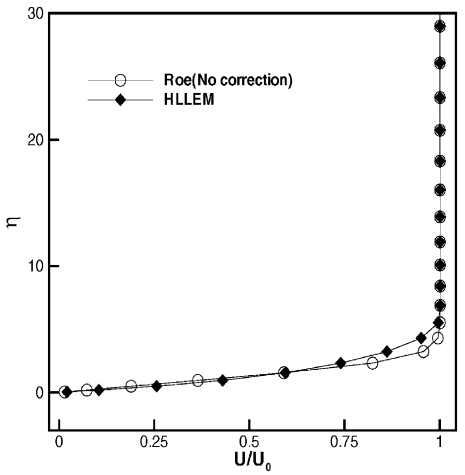

Fig. 3. Comparison of the second-order Roe and HLLEM for $M_\infty = 0.3$ laminar boundary layer.

Lemma 3.1 (Liou's lemma). *The exact solution of the Riemann problem for a* 1*-D contact discontinuity moving with speed* u_c *requires that*

$$D^{(\rho)} = |u_c|, \tag{21}$$

when $(u,p)_l = (u,p)_r = (u_c,p)$ and $\rho_l \neq \rho_r$.

As shown in this lemma, to resolve the stationary contact discontinuity exactly, the mass flux has to be removed when the Mach number goes to zero. By using Liou's lemma, it can be shown that the diffused HLLEM results are caused by the approximate speed of contact discontinuity. For clarity, we discuss the following corollary:

Corollary 3.1. *In order for* $D^{(\rho)}$ *of Godunov-type schemes to become* $|u_c|$, *g must be* 1 *when it is defined by*

$$g = \frac{|u_c| + a_c}{|\bar{u}| + a_c}. \tag{22}$$

Proof. Assuming $\rho_l \leqslant \rho_r$, the speeds of sound are related as $a_r \leqslant a_c \leqslant a_l$. It is easy to show that the Roe scheme exactly resolves the contact discontinuity. Roe scheme:

$$b^+ = \lambda_2 = u_c + a_c \quad \text{and} \quad b^- = \lambda_3 = u_c - a_c, \tag{23a}$$

$$D^{(\rho)} = |u_c| \quad \text{and} \quad g = 1. \tag{23b}$$

All Godunov-type schemes except the Roe have the same signal speeds

$$b^+ = \lambda_2 = u_c + a_c, \quad b^- = \mathbf{C}^- = u_l - a_l. \tag{24}$$

Then, we can show

$$D^{(\rho)} = \frac{1}{a_c + a_l}[|u_c|\{(2g-1)a_c + a_l\} + 2(1-g)a_c a_l|. \tag{25}$$

As a result, $D^{(\rho)} = |u_c|$ only if g is 1. □

The HLLE scheme in which g is zero shows the lowest accuracy since the mass flux remains when the Mach number goes to zero. It is natural that the HLLE contaminates solutions since it essentially has no consideration to contact discontinuity. The HLLEM scheme in which g is not one is not exact for the stationary contact discontinuity because of the use of Eq. (13). In the HLLEM scheme, the approximate speed of contact discontinuity produces unwanted diffusion to the linear degenerated fields. The Roe-averaged $|\hat{u}|$ must be used as the approximate speed of contact discontinuity when the anti-diffusive term is composed of the Roe eigenvectors, i.e.,

$$|\bar{u}|_{\mathrm{HLLEM}} = |\hat{u}|. \tag{26}$$

If we define the speed of the HLLEM scheme with Eq. (26), the resulting scheme can capture the stationary contact discontinuity exactly. It will be displayed in Fig. 9.

3.2. Signal speeds in expanding region

Generally, the nonlinear waves govern the behavior of the rarefaction waves as well as the shock. For the Roe scheme, rarefaction waves are regarded as discontinuity at the sonic point in the expanding region since it does not consider the entropy condition. The condition is automatically satisfied for the HLL solvers which have different numerical signal speeds from the Roe scheme. Fig. 4 shows that the solutions of a Riemann problem where the states $\mathbf{w}_l$ and $\mathbf{w}_r$ are connected by a rarefaction wave in the expanding region. The simple entropy correction for the Roe scheme, as shown, only reduces the strength of expansion shock. The HLL solvers give the same results and break up the initial discontinuity since they have the same numerical signal speeds.

The interesting problem concerned with rarefaction waves is the "receding flow problem." The solution consists of two rarefaction waves moving away from each other. Einfeldt et al. [6] considered the particular receding flow in which Roe's scheme broke down after a few time steps. They expressed the breakdown by

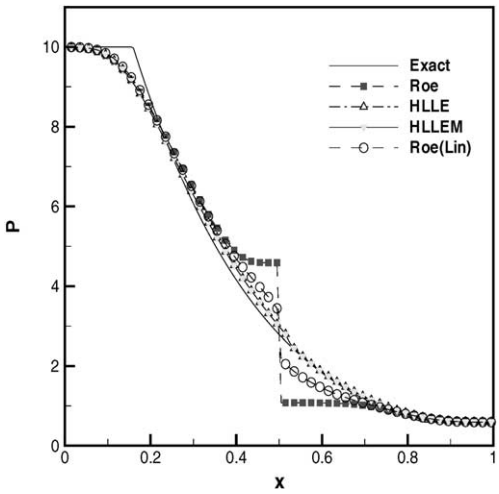

Fig. 4. Nonphysical expansion shock at the region expanding with initial condition $(\rho, u, p)_l = (1.205, 0, 10)$ fixed.

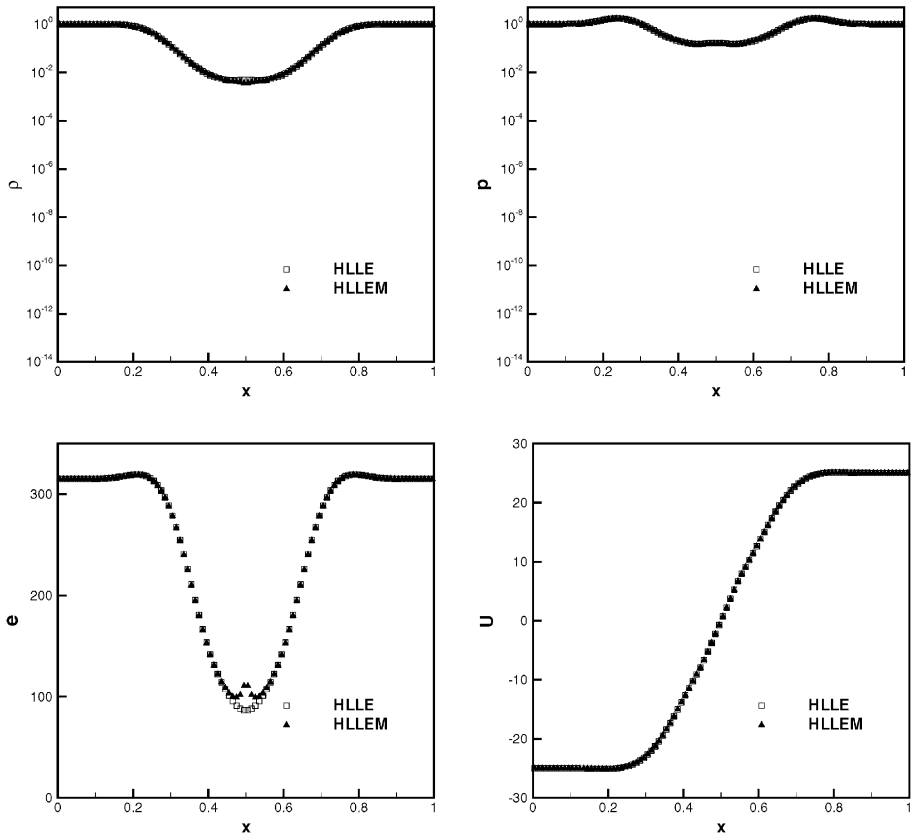

Fig. 5. The HLLE and HLLEM solutions for receding flow: $M_r = 25$, $M_l = -25$.

saying that certain Riemann problems are not linearizable. The reason for the failure of the Roe linearization is indeed the occurrence of two rarefaction waves in the exact solution to the Riemann problem [16].

For the case of a receding speed of Mach number of 25, the positively conservative HLLE scheme displays greatly smeared solutions near $x = 0.5$ where the speed vanishes, as shown in Fig. 5. In this nonlinearizable problem, the density and the pressure have to reach machine-zero values while the total energy maintains the initial condition. Despite that the HLLEM scheme is not positively conservative, it displays similar results and retains the positivity for this problem [8].

In view of physics, the vacuum state at the center interface means no flux, i.e., no fluid convection and wave interaction. This implies that the density and the pressure can reach machine-zero values only if the numerical convective flux vanishes at a vacuum state. Therefore, a numerical scheme has to be designed so that numerical solutions progress toward a physical vacuum state. We define this numerical property as the "vacuum preserving property."

Definition 3.1. A numerical scheme which preserves the initial vacuum condition has a vacuum preserving property.

It is found that the fluxes in the form of flux vector splitting such as the AUSM [8] and Van Leer [17] have vacuum preserving property according to the definition. However, the HLLE and HLLEM as well as

the Roe [1] and Osher and Solomon [2] do not have this property. To investigate the vacuum preserving property, the initial vacuum condition is given at center interface, i.e., $x = 0.5$. The following result can then be derived:

Lemma 3.2. A numerical flux function which can preserve an initial vacuum condition consists only of the pressure flux which is denoted by $\mathbf{f}^p = [0, p_{r=l}, 0]^{\mathrm{T}}$ in one dimension. Accordingly, the Godunov-type schemes do not preserve a vacuum state.

Proof. We begin by introducing two point states of the receding flow, where $\mathbf{w}_r = (\rho, \rho u, \rho e)$, $\mathbf{w}_l = (\rho, -\rho u, \rho e)$ and let $u_r = u > 0$, large enough to make a flow state vacuum. The Roe-averaged velocity at the interface is zero and the signal speeds b^+ and b^- of the HLL solvers are as follows:

$$b^+ = u_r + a_r = u + a, \quad b^- = u_l - a_l = -u - a. \tag{27}$$

Since the anti-diffusion term vanishes, all fluxes become HLLE flux. The pressure flux is extracted out of the original flux form such as by AUSM flux treatment [9] and then

$$\mathbf{f}(\mathbf{w}_l, \mathbf{w}_r) = \frac{b^+ u_l \mathbf{w}_l - b^- u_r(\mathbf{w}_r)}{b^+ - b^-} + \frac{b^+ b^-}{b^+ - b^-}(\mathbf{w}_r - \mathbf{w}_l) + \frac{b^+ \mathbf{f}^p - b^- \mathbf{f}^p}{b^+ - b^-} = \frac{a}{2}[\mathbf{w}_r - \mathbf{w}_l] + \mathbf{f}^p. \tag{28}$$

For the Roe scheme, the numerical flux in the vacuum condition can be shown as

$$\mathbf{f}(\mathbf{w}_l, \mathbf{w}_r) = \frac{u - a}{2}[\mathbf{w}_r - \mathbf{w}_l] + \mathbf{f}^p. \tag{29}$$

As can be seen, the momentum flux inevitably has remaining terms in the case of the receding flow, although the mass flux vanishes. □

The procedure of the proof shows that spurious and excessive dissipation to the momentum fluxes results from the forward and backward nonlinear waves. The excessive dissipation can be removed by forcing the numerical signal speeds of the waves to vanish. We define HLLEω scheme as an HLLE scheme with the following numerical signal speeds:

$$\mathbf{C}^+ = u_r + \omega \cdot a_r, \quad \mathbf{C}^- = u_l - \omega \cdot a_l, \tag{30}$$

$$\omega = \begin{cases} 1.0 & \text{if } M_l M_r \leqslant -1.0, \\ 0.0 & \text{otherwise.} \end{cases}$$

The HLLEω eliminates the transmission of the speed of sound by letting ω zero. In Fig. 6, the HLLEω solution displays the machine-zero density and discontinuity of the velocity in the vacuum state. Note that ω activates only for the supersonic receding flows.

Since the characteristics of the rarefaction waves are involved with the nonlinear signal speeds, the present Lemma 3.1 has consistency with Einfeldt's expression [6] for the nonexistence of the receding flows. The Godunov-type schemes are devised with the assumption that the forward and backward nonlinear waves, b^r and b^l, always exist in the approximate solutions of Riemann problems. So the schemes intrinsically impose a fundamental problem. As a result, the nonlinear waves must carefully be modified to preserve the vacuum states in the framework of the Godunov-type schemes.

Although the signal speeds of the HLLE help the scheme preserving positivity, they give dissipative momentum fluxes and do not preserve the vacuum states. On the other hand, the remaining terms of the Roe seem to be too large to keep the bound of positivity and may lead to the negative internal energy. It is somewhat ambiguous what relation exists between the positivity and the vacuum preserving property of any scheme. More study to assess this relation is definitely needed.

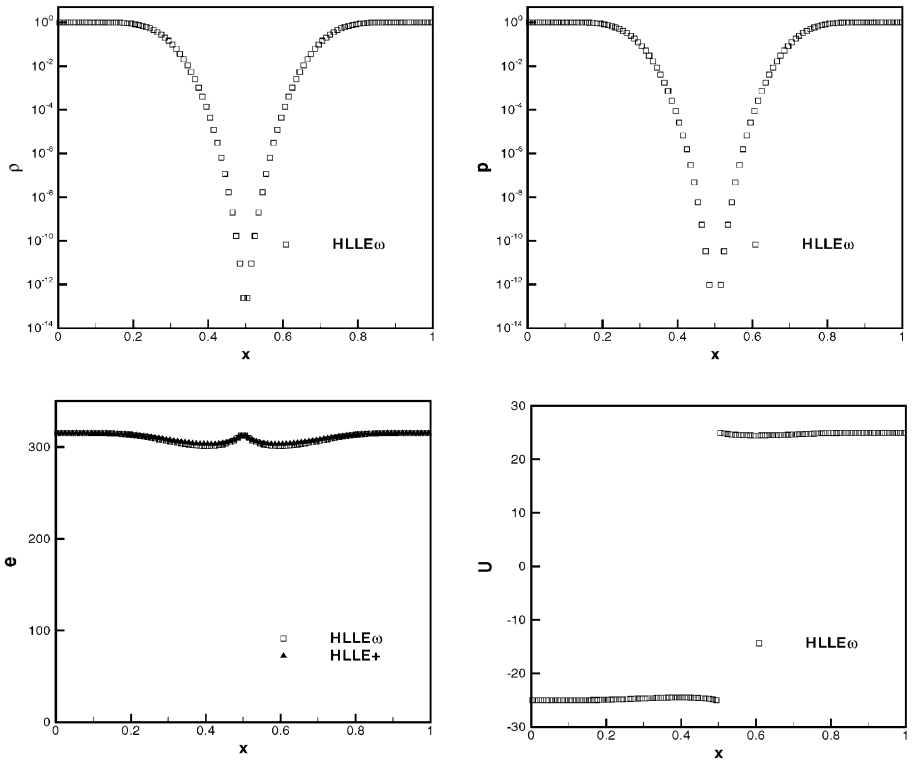

Fig. 6. The HLLEω solution for receding flow: $M_r = 25$, $M_l = -25$.

3.3. Shock instability

It is well known that approximate Riemann solvers such as the Roe and the HLLEM occasionally fail to stabilize strong normal shocks, namely the carbuncle. The catastrophic phenomena occur only in multi-dimensional cases. Several researchers have considered the dynamics of the instability process as the "odd–even decoupling" process [11,18]. To investigate the problem, a normal shock moving in a long channel grid with a small saw-tooth perturbation is computed. In Fig. 7, the solutions of the Roe and the HLLEM schemes totally break the normal shock indicating an odd–even decoupling behavior. The HLLE, on the other hand, accurately preserves the initial normal shock even after a long time. Because the HLLEM scheme has a similar mechanism as with the Roe scheme on linear degenerated fields, it exhibits behavior like that of the Roe scheme [7]. Considering that the HLLE does not suffer from the breakdown, one may say that the anti-diffusion term of Eq. (7) is the numerical cause of the breakdown.

Quirk [11] performed a linear stability analysis for the Roe and the HLLE schemes and insisted that the catastrophic solution of the Roe scheme was caused by the coupling of pressure and density perturbations. On one hand, Liou discussed the dynamics of the instability process in terms of $D^{(p)}$ (shown in Eq. (20)) in the numerical mass flux. Furthermore, he discussed that a scheme having the property $D^{(p)} = 0$ in the mass flux is a "shock-stable" scheme. This discussion is equivalent to the analysis of Quirk's in that they all agree that the density perturbation coupled with pressure amplifies the instability in the transverse direction to the shock waves. We start from the assumption that Quirk's analysis is valid for tracing the mechanism of the instability. The detailed analysis through a unified representation of the Godunov-type schemes gives the following lemma.

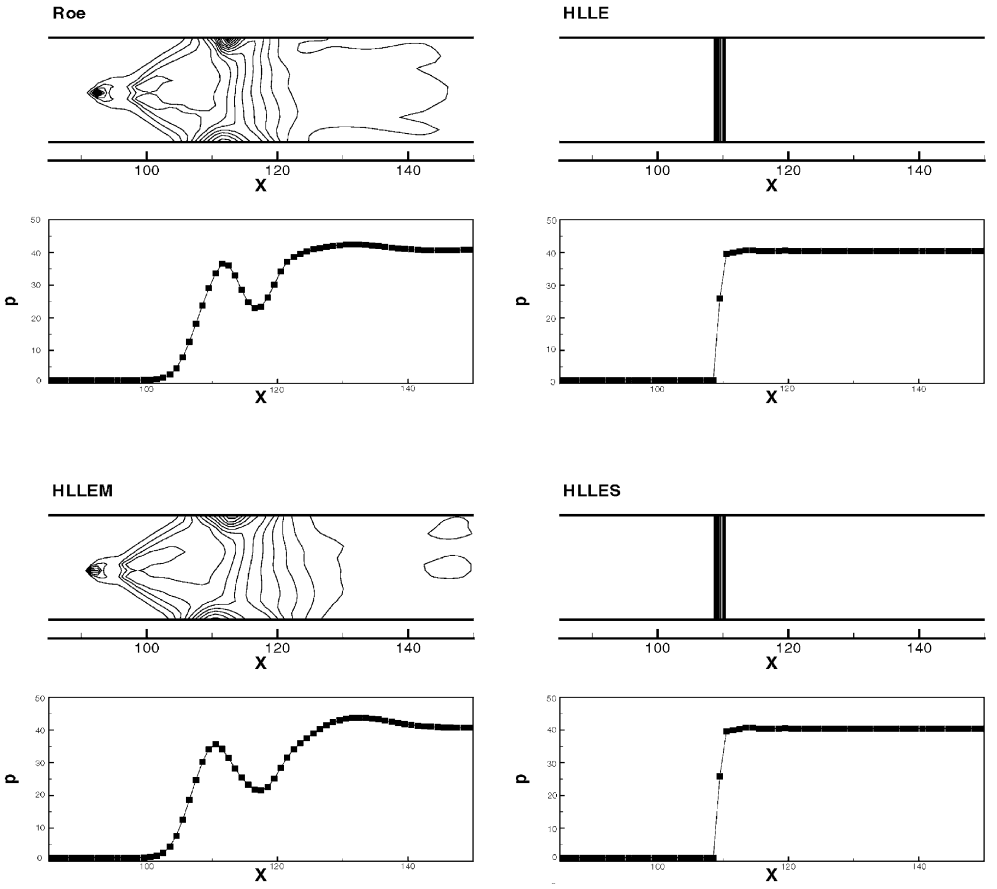

Fig. 7. Odd–even decoupling: $M_s = 6.0$.

Lemma 3.3. Define a shock-stable scheme such that it does not amplify the disturbances at the shock. In the framework of the Godunov-type schemes, $\bar{\delta} \neq 1$ if it is shock stable.

We assume that the 2-D computational mesh is uniform with small perturbations at the centerline, and that the discrete solution at time t^n is given by

$$\rho_j^n = \rho \pm \tilde{\rho}^n, \quad p_j^n = p \pm \tilde{p}^n, \quad u_j^n = u, v_j^n = 0,$$

as j is odd or even. Here $\tilde{\rho}^n$ and $\tilde{p}^n$ are the amplitudes of the perturbations for the density and pressure fields, respectively. If we consider the discretized equations, Eq. (4), the amplitude at n+1 time level may be manipulated to give

$$\begin{aligned} \tilde{\rho}^{n+1} &= (1 - 2v_y)\tilde{\rho}^n + 2v_y\bar{\delta}\left(\tilde{\rho}^n - \frac{\tilde{p}^n}{\hat{a}^2}\right), \\ \tilde{p}^{n+1} &= (1 - 2v_y)\tilde{p}^n. \end{aligned} \tag{31}$$

Making a loose approximation that $\hat{a}$ maintains constant, Eq. (31) becomes at the time level t^n with initial one-off perturbation $(\tilde{\rho}^0, \tilde{p}^0)$:

$$\tilde{\rho}^n = [1-2(1-\bar{\delta})v_y]^n\left(\tilde{\rho}^0 - \frac{\tilde{p}^0}{\hat{a}^2}\right),$$
$$\tilde{p}^n = (1-2v_y)^n\tilde{p}^0. \tag{32}$$

From this it can be seen that the initial perturbation to the pressure field is damped out if the Courant–Friedrichs–Levy (CFL) condition($v_y < 1$) is given. The density perturbation is damped out if

$$\bar{\delta} \neq 1. \quad \square \tag{33}$$

Eq. (32) shows that the value $\bar{\delta}$ is a dominant factor to determine whether the density perturbation damps out or not. Since the above analysis is based on a loose approximation, the condition $\bar{\delta} \neq 1$ may be the only necessary condition that odd–even decoupling does not exist in any cases. This analysis opens a possibility to suppress the instability even though a scheme has $D^{(p)} \neq 0$. To assess the lemma, an HLLE switched(HLLES) scheme is suggested with a switching mechanism:

$$|\bar{u}| = \beta\left|\frac{b^r + b^l}{2}\right| + (1.0-\beta)\hat{a}, \tag{34}$$

$$\beta = \begin{cases} 1.0 & \text{if } (k_p)_{ij} \leqslant 0.01, \\ 0.0 & \text{otherwise}, \end{cases} \tag{35}$$

where k_p is the shock indicator which is defined in Eq. (18). Note that the anti-diffusion coefficient $\bar{\delta}$ is one for the Roe and the HLLEM and zero for the HLLE. For the present HLLES scheme, the value of $\bar{\delta}$ is set to 0.5 since $|\bar{u}|$ becomes $\hat{a}$ when the switching is activated at the shock. As seen in Fig. 7 (bottom right), the instability does not occur. It is noted that if $\bar{\delta}$ is set to 0.5 the HLLES scheme does not have the property, $D^{(p)} = 0$. In other words, the results show that a shock stable scheme does not strictly require $D^{(p)} = 0$ although a scheme with $D^{(p)} = 0$ is always shock stable. If a scheme with $\bar{\delta} = 0.5$ does not have a switching mechanism, it is not suitable for the viscous computation since the boundary layer is contaminated by the excessive dissipation; see Section 3.1.

4. HLLE+ scheme

It is noted that the numerical dissipation mechanism can be understood mainly through the anti-diffusion terms which are explicitly identified [10]. This is important in constructing a new HLL solver which captures strong shocks without encountering shock instability nor contaminating the inherent resolution of the scheme in viscous flows. We propose a new shock stable method which improves the dissipation mechanism of anti-diffusion terms. For brevity, it is denoted by HLLE+ in this paper.

Present HLLE+ scheme:

$$\mathbf{C}^+ = u_r + a_r, \quad \mathbf{C}^- = u_l - a_l, \tag{36a}$$

$$|\bar{u}| = \beta|\hat{u}| + (1.0-\beta)\hat{a}. \tag{36b}$$

$$\beta = \begin{cases} 1.0 & \text{if } (k_p)_{ij} \leqslant \beta^*, \\ 0.0 & \text{otherwise}, \end{cases} \tag{37}$$

where β^* is a constant between 0.01 and 0.1. A switching parameter β is introduced to reduce the value of the anti-diffusion coefficient $\bar{\delta}$ in the vicinity of some instabilities. It is noted that $\bar{\delta}$ is set to 0.5 if the

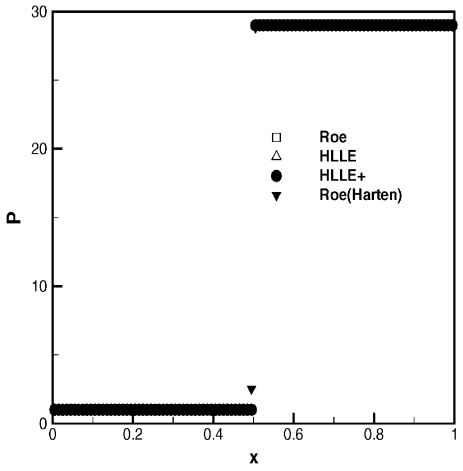

Fig. 8. Normal shock discontinuity: $(\rho, u, p)_l = (1, 5.916, 1)$ and $(\rho, u, p)_r = (5, 1.183, 29)$ at center.

switching is activated. Quirk [11] proposed a switching method based on the pressure gradient. Quirk used the HLLE scheme as an alternate method when the base was the Roe scheme. The main difference of the present scheme compared to Quirk's method is that the switching is based on the second derivative of pressure. According to our numerical experiments, the second derivative-based scheme is more robust than that based on the first order one. Thus it can reduce or even eliminate the dependency on the grid and the flow conditions. Since it is found that the accuracy of the scheme is not sensitive to β^*, the value is fixed to 0.01 in the following numerical results.

Fig. 8 shows the results for the single normal shock discontinuity. All schemes produce the exact solution except the Roe with the entropy correction which resolves the shock with two intermediate points. The Harten correction, $\epsilon^* = 0.25$, is used here. The corrections for the Roe, essential in preventing shock instability, degrade the accuracy of shock discontinuity. Although the switching function of the HLLE+

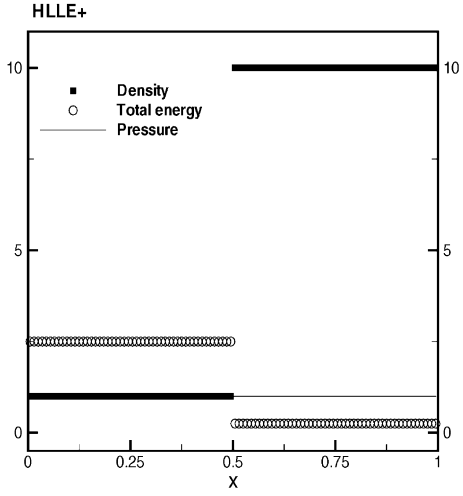

Fig. 9. The HLLE+ solution for the stationary contact discontinuity.

scheme is activated mostly near shock discontinuity, the resolution of the shock discontinuity is preserved. In other words, switching scheme like the HLLE+ scheme can remove some instability by changing the dissipation mechanisms without degrading accuracy. This is the reason that we favor switching the intrinsic dissipation rather than limiting the amount of the dissipation.

As a consequence of the Corollary 3.1, the approximate speed of the contact discontinuity is proposed as Eq. (36b) in order to accurately resolve the contact discontinuity. In Fig. 9, displayed is the HLLE+ solution for the stationary contact discontinuity which has the same initial conditions as Fig. 2. As expected, the HLLE+ scheme gives exact solutions. The dramatic improvement by the HLLE+ scheme is due to the approximate speed of contact discontinuity. The boundary layer solutions are also regenerated to compare the numerical dissipation of each scheme. As seen in Fig. 10, the Roe and the HLLE+ schemes agree very well with the Blasius analytic solution. It is natural that the HLLE displays a much diffused result. The HLLE+ solutions indicate that it can accurately capture viscous boundary layer as well as stationary

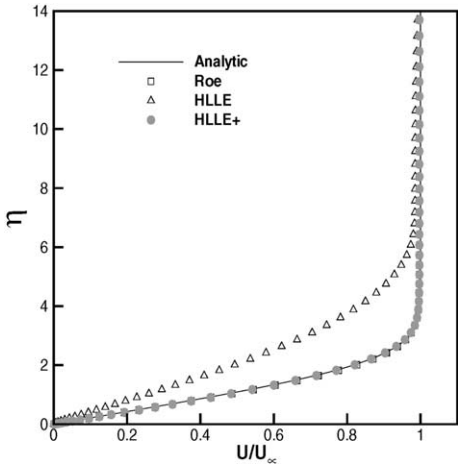

Fig. 10. Effect of numerical dissipation of Roe, HLLE and HLLE+ for laminar boundary layer: $M_\infty = 0.3$.

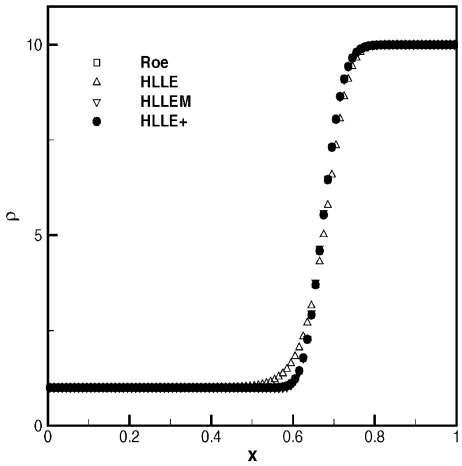

Fig. 11. Moving contact discontinuity: $(\rho, u, p)_l = (0.125, 0.1125, 1)$ and $(\rho, u, p)_l = (10, 0.1125, 1)$ as initial conditions at center.

Table 1
Blunt body grid systems

Grid	Size	CRN (cell Reynolds number)	
A	65×65	2	
B	65×65	57	
C	33×33	114	Double spacing of Grid *B*

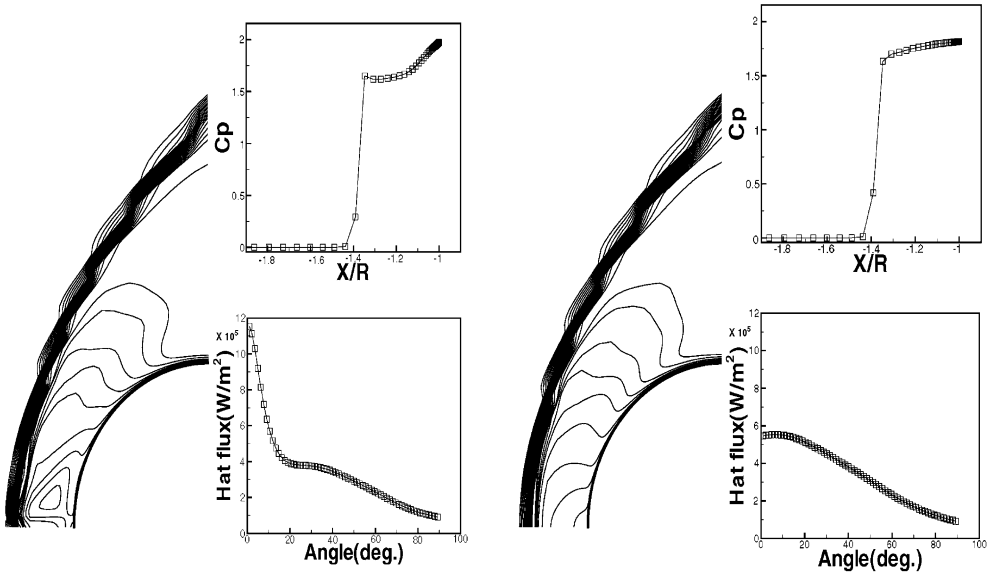

Fig. 12. Mach number contour, C_p distribution and wall heat fluxes for the flow past a blunt body with $M_\infty = 16.34$: (left) Carbuncle phenomenon of the original HLLEM, (right) HLLE+ solution with contaminated HLLEM solution as initial condition.

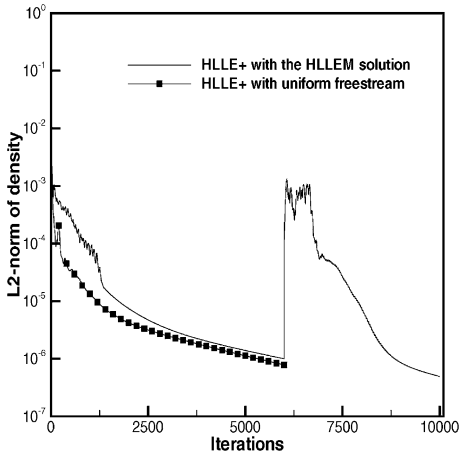

Fig. 13. Convergence history of HLLE+ solution with the HLLEM solution and freestream as the initial conditions for $M_\infty = 16.34$ blunt body flows.

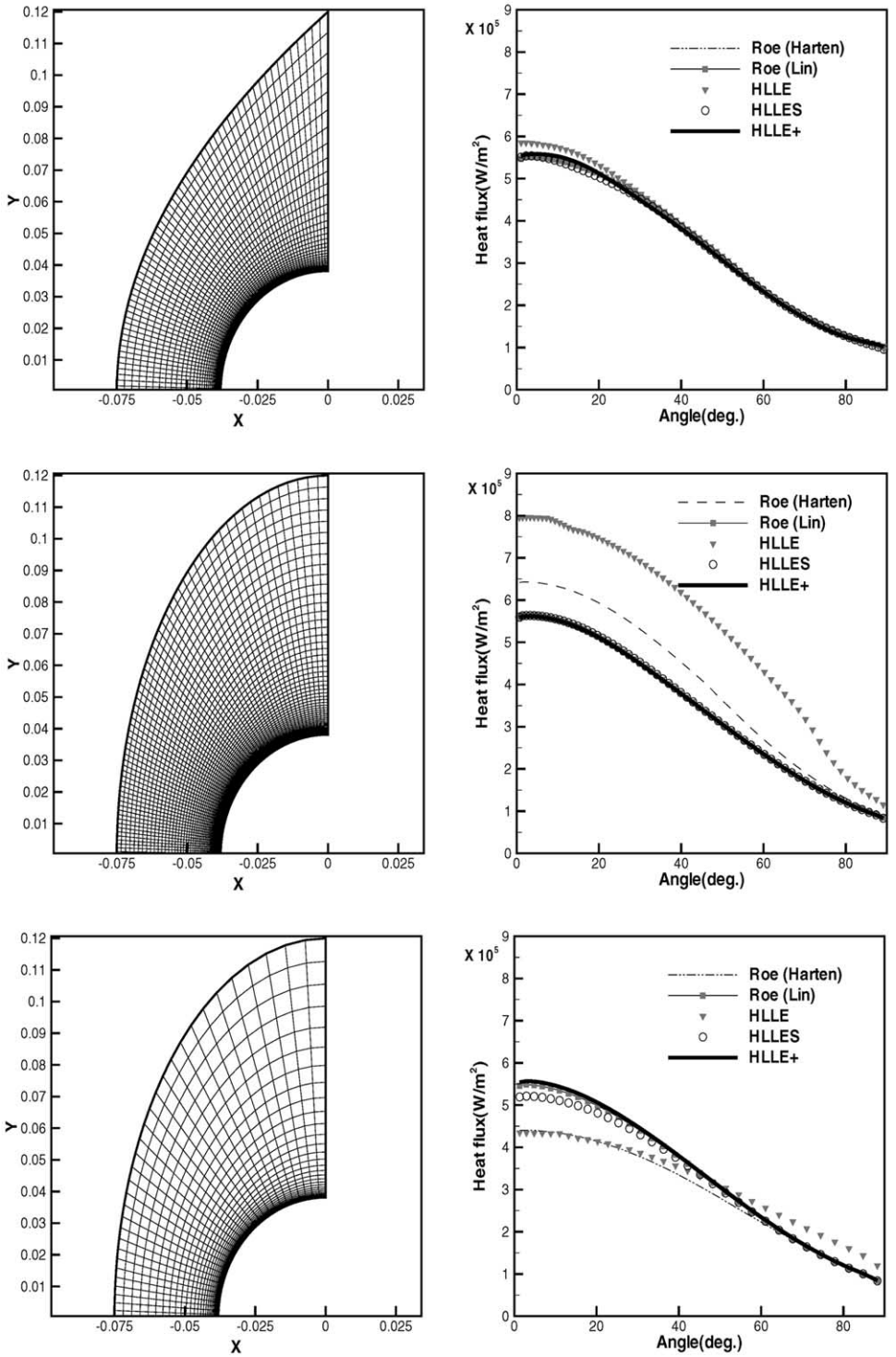

Fig. 14. Grid and heat fluxes on $M_\infty = 16.34$ blunt body: (top) CRN = 2, (middle) CRN = 57, (bottom) CRN = 114.

contact discontinuity. Similarly, each of the Godunov-type schemes has the same dissipation mechanism for the moving contact discontinuity. The HLLE scheme has the poorest resolution as shown in Fig. 11. The difference among other schemes is too small to distinguish.

To investigate the effect of the numerical dissipation on the accuracy for viscous problem, a 2-D hypersonic viscous flow past a cylinder is presented. The freestream conditions are as follows: $M_\infty = 16.34$, $T_\infty = 52$ K, and $Re/m = 3.94 \times 10^6$. The cylinder radius is $0.0381m$ and $T_{\text{wall}} = 294.4$ K. The conditions represent a low enthalpy flow which is used for the validation of hypersonic flows under perfect gas approximation [19]. Three sets of grid systems, as shown in Table 1, are tested to verify the grid dependency of each scheme. The surface cell Reynolds numbers (CRN) at the stagnation point of each grid are about 2, 57 and 114, respectively. Grid C is made by double spacing of grid B in each direction.

At the surface the no-slip and constant temperature wall boundary conditions are applied. The specified freestream conditions are enforced for inflow boundary conditions and zero-order extrapolations at outflow boundary are applied. To obtain second-order accuracy, the MUSCL interpolation method is used with the minmod limiter which degrades the accuracy to be first-order at strong discontinuities [15]. The diagonalized alternating direction implicit (DADI) method [20] is used to obtain the steady solutions. Coakley's modified approach [21] for the DADI algorithm is applied to reduce the stiffness of viscous fluxes. Further descriptions can be found in the literatures.

Fig. 12 displays the Mach number contour, C_p distributions along the stagnation streamline and wall heat fluxes on the surface of the HLLEM and HLLE+ schemes on the highly stretched grid A when the CFL number is 1.5. The contaminated HLLEM solution (left) is obtained at 6000 iterations. The spurious vortical stream is thought of as an example of the carbuncle phenomenon at hypersonic viscous flows. The "self-correcting" solution [9] (right) are obtained with the shock-stable HLLE+ scheme after 6000 iterations. It is interesting that the original HLLEM solution converges to an odd steady state which predicts a much higher heat fluxes. The convergence history in Fig. 13 also shows that the HLLE+ scheme continued with the odd HLLEM solution has nearly the same convergence rate with the computation using the uniform freestream condition as the initial condition.

Fig. 14 shows the used grids and the computed surface heat fluxes with CRN 2, 57 and 114, respectively. All computations are converged to 10^{-6} for the L2-norm of density which is enough to converge below 10^{-4} of the heat fluxes. As shown in right figures of Fig. 14, the HLLE+ scheme shows good agreement with Fay and Riddell's theoretically predicted value [22] of 5.6×10^5 W/m^2 for all grids. The HLLE scheme also gives a highly dissipative solution for high CRN. For the Roe scheme with the Harten correction, it makes the boundary layer dissipative as the CRN of the grid increases. In this case, $\epsilon^* = 0.25$ is used for preventing the carbuncle. The Roe with the Lin correction is not sensitive to grid spacing since its numerical dissipation does not contaminate the boundary layer. This result shows that the Roe scheme can be sensitive to grid spacing according to the mechanism of the entropy correction functions. The HLLES scheme gives more dissipative solutions than the HLLE+ as shown in Fig. 14 (bottom). This difference between HLLES and HLLE+ results from the difference of the definitions for the approximate speed of the contact discontinuity. The results also show that the additional numerical dissipation within the boundary layer of hypersonic viscous flows precludes accurately computing the wall heat fluxes.

5. Concluding remarks

A unified representation with control parameters provides significant information about the accuracy and robustness of the Godunov-type schemes. To eliminate the erroneous diffusion of HLLEM scheme, we showed that the Roe-averaged $|\hat{u}|$ must be used as the approximate speed of contact discontinuity when the anti-diffusive term is composed of the Roe eigenvectors. As a consequence of the analysis for the vacuum preserving property, we also suggested that the diffused solutions of the strong receding flow result from the

numerical signal speeds of the Godunov-type schemes fundamentally. A shock stable HLLE+ scheme with nonzero $D^{(p)}$ in the mass flux was proposed. The HLLE+ scheme, which successfully eliminates the erroneous dissipation and the instability of the HLLEM scheme, accurately predicted the surface heat fluxes without grid dependency.

References

[1] P.L. Roe, Approximate Riemann solvers, parameter vectors and difference schemes, J. Comput. Phys. 43 (1981) 357.
[2] S. Osher, F. Solomon, Upwind difference schemes for hyperbolic systems of conservation laws, Math. Comput. 38 (1982) 339.
[3] S.K. Godunov, A difference scheme for numerical computation of discontinuous solutions of equations of fluid dynamics, Math. Sbornik. 47 (1959) 271.
[4] A. Harten, P.D. Lax, B. van Leer, On upstream differencing and Godunov-type schemes for hyperbolic conservation laws, SIAM Rev. 25 (1983) 35.
[5] B. Einfeldt, On Godunov-type methods for gas dynamics, SIAM J. Numer. Anal. 25 (1988) 294.
[6] B. Einfeldt, C.D. Munz, P.L. Roe, B. Sjögreen, On Godunov-type methods near low densities, J. Comput. Phys. 92 (1991) 273.
[7] S. Obayashi, Y. Wada, Practical formulation of a positively conservation scheme, AIAA J. 32 (1993) 1093.
[8] M.-S. Liou, Probing numerical fluxes: mass flux, positivity, and entropy-satisfying property, AIAA paper 97-2035-CP (1997).
[9] M.-S. Liou, Mass flux schemes and connection to shock instability, J. Comput. Phys. 160 (2000) 623.
[10] S.H. Park, J.H. Kwon, Study of Godunov-type schemes using control parameters, in: Proceedings of 4th Asian CFD Conference, Mianyang, China, 2000, p. 574.
[11] J.J. Quirk, A contribution to the great Riemann solver debate, Internat. J. Numer. Methods Fluids 18 (1994) 555.
[12] S.H. Park, J.H. Kwon, An improved HLLE method for hypersonic viscous flows, AIAA paper 2001-2633 (2001).
[13] A. Harten, High resolution schemes for hyperbolic conservation laws, J. Comput. Phys. 49 (1983) 357.
[14] H.-C. Lin, Dissipation additions to flux-difference splitting, J. Comput. Phys. 117 (1995) 20.
[15] W.K. Anderson, J.L. Thomas, B. van Leer, Comparison of finite volume flux vector splittings for the Euler equations, AIAA J. 24 (1986) 1453.
[16] R. Donat, A. Marquina, Capturing shock reflections: an improved flux formula, J. Comput. Phys. 125 (1996) 42.
[17] B. van Leer, Flux-vector splitting for the Euler equations, in: Lecture Notes in Physics, vol. 170, Springer, Berlin, 1982, p. 507.
[18] K.M. Peery, S.T. Imlay, Blunt-body flow simulations, in: AIAA/SAE/ASME/ASEE 24th Joint Propulsion Conference (AIAA paper 88-2904), 1988.
[19] D. Gaitonde, J.S. Shang, Accuracy of flux-split algorithms in high-speed viscous flows, AIAA J. 31 (1993) 1215.
[20] T.H. Pulliam, D.S. Chaussee, A diagonal form of an implicit approximate factorization algorithm, J. Comput. Phys. 39 (1981) 347.
[21] T.J. Coakley, Implicit upwind methods for the compressible Navier–Stokes equations, AIAA J. 23 (1984) 374.
[22] J. Fay, F. Riddell, Theory of stagnation point heat transfer rate in dissociated air, J. Aeronaut. Sci. 25 (1953) 73.